ISC/23/SHARKWG-1/2

Spatio-temporal model for CPUE standardization: Application to shortfin mako caught by Japanese offshore and distant water shallow-set longliner in the western and central North Pacific[1]

Mikihiko Kai[2]

[2]Fisheries Resources Institute, Highly Migratory Resources Division,
Japan Fishery Research and Education Agency
2-12-4 Fukuura, Kanazawa, Yokohama, Kanagawa 236-8648, JAPAN
Email: kai_mikihiko61@fra.go.jp

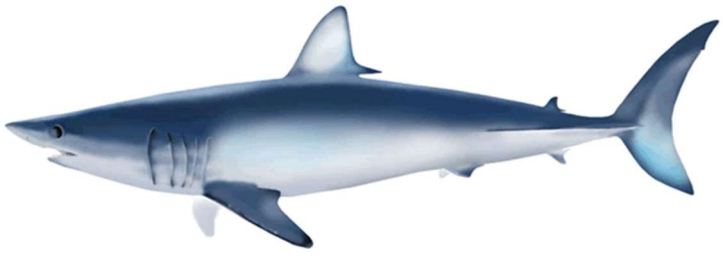

[1] Working document submitted to the ISC Shark Working Group Workshop, 29-30 November- 1-2, 4-7 December 2023, Yokohama, Kanagawa, Japan. **Document not to be cited without author's permission.**

Abstract

This working paper provides a standardized CPUE of shortfin mako, *Isurus oxyrinchus*, caught by Japanese offshore and distant-water shallow-set longline fishery from 1994 to 2022 in the western and central North Pacific Ocean. Since the catch data of sharks caught by commercial tuna longline fishery is usually underreported due to discard of sharks, the author filtered the logbook data using the simple filtering methods applied to the blue shark in the previous analysis. The nominal CPUE of filtered shallow-set data was then standardized using the spatio-temporal generalized linear mixed model (GLMM) to provide the annual changes in the abundance of shortfin mako in the northwestern Pacific. The author focused on seasonal and interannual variations of the density in the model to account for spatially and seasonally changes in the fishing location due to the target changes between blue shark and swordfish. The estimated annual changes in the CPUE of shortfin mako revealed an upward trend from 1994 to 2014, and then downward trend until 2020. Thereafter the CPUE slightly increased in recent years. The estimated CPUE trends from the spatio-temporal model with a large amount of data collected in the most abundant waters in the western and central North Pacific is a very useful information about the abundance of North Pacific shortfin mako.

Introduction

Shortfin mako, *Isurus oxyrinchus*, is widely distributed in the world oceans from temperate to tropical waters and commonly caught by bycatch of longline fishery targeting tunas, billfishes, and sharks. In the previous benchmark stock assessment in 2018, nominal CPUE of North Pacific shortfin mako caught by Japanese offshore and distant water shallow-set longline fishery for 1994-2016 was standardized using three generalized linear models (GLMs) after logbook data was filtered using two-step filtering methods (Kai, 2017). The three GLMs includes 1) negative binomial model, 2) zero-inflated negative binomial model and 3) zero-inflated Poison model. The zero inflated negative binomial model was selected using AIC and BIC as the most parsimonious model. The standardized CPUE of the best model was initially considered as a high priority for the full stock assessment in considering with the statistical soundness, long timespan, extensive spatial coverage, and relatively high catch rates (ISC, 2018). However, further explorations showed that the steep increasing trend of this index was inconsistent with all the other indices available, as well as biologically implausible given the understanding of shortfin mako's population dynamics at that time. Consequently, the International Scientific Committee for Tuna and Tuna-like Species in the North Pacific Ocean (ISC) SHARKWG determined not to include this index in the base case

model (ISC, 2018). The SHARKWG acknowledged insufficient analysis for an issue of the CPUE standardization on the targeting/fishing strategy shifts from blue shark to swordfish and vice versa. In addition, the author acknowledges that the two-stage filtering method for logbook data as well as design-based GLM analysis have a fundamental issue on the CPUE standardization.

The VAST (Vector Autoregressive Spatio-Temporal) software package for R (Thorson, 2019), which enables us to analyze fishery data using the spatio-temporal generalized linear mixed model (GLMM) (Thorson, 2019), has attracted attention as a novel approach and is now commonly used globally to predict spatial changes in species distribution and temporal variations in a population range and density. The basic model structure of VAST adopts a delta-GLMM which can consider spatio-temporal correlations among categories such as a species. Indeed, the spatio-temporal model was applied to the estimation of abundance from multi-species fishery data accounting for spatio-temporal variation and fisher targeting (Thorson et al. 2017). This fact implies that the multispecies spatio-temporal model has a high potential to improve the CPUE standardization of the shortfin mako caught by Japanese shallow-set longline fishery in the western and central North Pacific. However, the multiple reports from the Japanese skipper's notes revealed that the Japanese shallow-set longline fleets only changed their operational area by season without changing the gear configurations (e.g., hooks between floats and length of the blanch line) even if they changed their target species. The main reason why the previous authors (Hiraoka et al., 2016; Kai and Shiozaki, 2016; Kai, 2017) directly considered the target effects in the CPUE standardization is that the GLM commonly requires to provide a spatial area with a low resolution (e.g., four areas) in the analysis. Therefore, they directly included the target effect in the model as it was impossible to directly explain the spatio-temporal changes in the operational area using the GLM. If a single-species spatio-temporal model can account for the seasonal and interannual variation in the spatial changes of the density with higher spatial resolutions, it is reasonable to use the spatio-temporal model for the CPUE standardization without directly considering the target effect in the analysis. Recently, Thorson et al. (2020) developed such a model and Kai (2021) applied the model to the North Pacific blue shark, *Prionace glauca*.

The objective of this working paper is to estimate the standardized CPUE of shortfin mako caught by Japanese offshore and distant-water shallow-set longline fishery for 1994-2022 using the spatio-temporal GLMM in consideration with seasonal and interannual changes in

the density.

Materials and Methods

Data sources

Set-by-set logbook data 1994 to 2022 from Japanese offshore and distant water longline fishery were used. Set-by-set data used in this study included information on catch number, amount of effort (number of hooks), number of branch lines between floats (hooks between floats: HPF) as a proxy for gear configuration, location (longitude and latitude) of set by resolution of 1 × 1 degree square, vessel identity, fishery type (offshore or distant water), and the prefecture in Japan where the longline vessels were registered. The offshore-water fleet was defined by tonnage of vessels between 20 and 120 MT, while the distant-water fleet consisted of vessels larger than 120 MT. The four seasons (quarters (Q) 1 to 4) of the year were defined as follows: Q1 was spring from January to March; Q2 was summer from April to June; Q3 was fall from July to September; and Q4 was winter from October to December.

Simple data filtering

To remove set-by-set logbook data of mis- and under- reporting or discarding for pelagic sharks, simple data filtering method was employed. The data was filtered by 1) type of fishery and size of vessel (Japanese offshore and distant-water commercial longliner with more than 20 vessel tonnage: “Enyo and Kinkai” fisheries), 2) reporting ratio of pelagic sharks by cruise (more than 94.6%), 3) registered prefectures ("Tohoku, Hokkaido and Toyama" regions), 4) depth of gear-setting (i.e., number of hooks between floats; HBF: 3~5) and 5) temperate water in the western and central North Pacific Ocean (north of 20°N and west of 160°W). The data filtered by these conditions has a characteristic that the fleets target pelagic sharks such as a blue shark, *Prionace glauca,* in the western and central North Pacific Ocean, and the fleets land shortfin mako at the Japanese fishing ports. This simple data filtering was justified through comparing with the annual trends in nominal CPUE of shortfin mako caught by “Kesennuma” fleets (see Kai, 2023).

CPUE standardization with spatio-temporal model

The spatio temporal model was consisted of two components of encounter probability and positive catch in a delta model. The first predictor was modeled using a binomial model to account for the encounter probability (mean positive catch rate = 55 %), however, only the intercept (constant for all year) was considered in the model due to the issue of convergence

for the random effect model. Second predictor was modeled using a negative binomial (NB) model to account for the count data with over-dispersion (variance/mean =8.8):

$$c \sim NegBin\ (c^*, c^*(1+\sigma_1) + c^{*2}\sigma_2),$$
$$\log\ (d) = d_0(t) + \gamma(s) + \omega(s,q) + \delta(s,y) + \theta(s,t), \quad (1)$$

where c is observed catch, *NegBin* (a, b) is a negative binomial distribution with mean a and variance b (Lindén and Mäntyniemi, 2011), c^* is an expected catch and a function of density d and fishing effort f (number of hooks = 1), σ_1 and σ_2 are residual variations, $d_0(t)$ represents temporal variation (the intercept for each year-season t), $\gamma(s)$ represents spatial variation (s), $\omega(s,q)$ represents spatio-temporal variation (station s and season q), $\delta(s,y)$ represents spatio-temporal variation (station s and year y), and $\theta(s,t)$ represents spatio-temporal variation (station s and year-season t). The intercept $d_0(t)$ were decomposed into season and year main effects and an autocorrelated interaction of season and year were used to specify the interpolation for season-year combinations (Thorson et al., 2020).

The VAST (v3.10.1) was used to standardize the nominal CPUE. Temporal abundance index I was estimated as:

$$I(t) = \sum_{s=1}^{n_s} f(s) \times c^*(s,t) / \{\sum_{t=1}^{n_t} \sum_{s=1}^{n_s} f(s) \times c^*(s,t)\}, \quad (2)$$

where n_s is total number of knots at location s. The number of knots (n_s = 100) was specified in a balance between computational speed and spatial resolution.

Model selection and diagnostics

To select the best model, the explanatory variable was sequentially added to the year-season random effect model. The best model was selected using the AIC (Akaike, 1973) and BIC (Schwarz, 1978). Given the different model is selected by AIC and BIC, the model selected by BIC is chosen to avoid the overfitting that the AIC tends to choose the complex model with a lot of data (Shono, 2005). For the best model, the goodness of fits was examined using the Pearson residuals and QQ-plot. The residuals were computed using a randomized quantile (Dunn and Smyth, 1996) to produce continuous normal residuals.

Results

Simple data filtering reduced the number of datasets (i.e., set-by-set data for 1994-2022) collected in the North Pacific Ocean from 1,887,951 to 119,177.

Selection of the best model

All models were reasonably converged with the positive definite of hessian matrix and a small value of maximum gradient (**Table 1**). The model (M-3) including spatial (station) and spatio-temporal variances (season and station, and year-season and station) as random effects was identified by BIC as the most parsimonious model (**Table 1**). The estimated CPUE changed substantially if random effect component of year and station was added to the simple model (M_4, 5) (**Fig. 1**). Diagnostic plots of goodness-of-fit for the best model didn't show serious deviations from normality and model misspecification (**Fig. 2**). These results suggested that the fitting of the best model to the data was good. Lists of all parameters and estimates of the best models are shown in **Table 2**.

Temporal trends in CPUE

The estimated annual changes in the CPUE of shortfin mako revealed a continuous upward trend from 1994 to 2014, and then gradually downward trend until 2020. Thereafter the CPUE slightly increased in recent years (**Fig. 3**). The 95% confidence intervals of the CPUEs were larger after 2011 (**Fig. 3**) due to the decline of fishing effort (**Table 3**; **Fig. A1**). The estimated seasonal changes in the CPUE of shortfin mako indicated the highest CPUE in Q4 and followed by that in Q2, Q3 and Q1 (**Fig. 4**). Temporal (year-season) changes in the distribution shift, range expansion, and predicted CPUEs are shown in **Appendix**.

Spatiotemporal trends in CPUE

Overall, there were sort of spatiotemporal patters of predicted CPUEs of shortfin mako throughout the year-season spatial maps (**Figs. 5-7**). The higher CPUEs (hotspots) of shortfin mako were observed in the waters of coastal area of Japan (30-40°N, 140°-150°E) in Q2 and Q3 (e.g., Q2 in 1997, Q3 in 2001, Q2 and Q3 for 2010-2012, Q2 for 2014-2019 etc.) and offshore area of Japan (30-45°N, 140°-160°E) in Q3 and Q4 (e.g., Q3 in 2003, Q4 for 1999-2001, Q4 after 2009 etc.) In addition, the higher CPUEs of shortfin mako were also observed in the water at the lower latitude (25-35°N, 140°-180°E) in Q1 (e.g., 1996-2003, 2013 and 2014 etc.). The hotspots of shortfin mako were substantially changed by year (**Fig. 8**), while those were not largely changed by season (**Fig. 9**). The higher CPUEs were observed in the Kuroshio-Oyashio transition zone (TZ) (32-42°N, 160°E -160°W) for the whole seasons, while the lower CPUEs of shortfin mako were observed in the sub-tropical area (25-35°N, 138°-170°E) except for winter in Q4 (**Fig. 9**).

Discussions

This document paper estimated a historical trend in abundance indices of shortfin mako caught by Japanese shallow-set longline fishery in the western and central North Pacific Ocean from 1994 to 2022 using a spatio-temporal GLMM in considerations with seasonal and interannual variations of the density. The main advantage of the spatio-temporal model is an imputation for the missing data using spatial and temporal correlations through random effects (Thorson, 2019). Unlike the design based GLM used in the previous assessment (Kai, 2017), the spatio-temporal GLMM developed by Thorson et al. (2020) enabled us to include interaction terms between spatial and temporal effects (season, year, and season-year effects) with high spatial resolutions. The spatio-temporal variations with high spatial resolution had a large impact on the seasonal trends in the estimated CPUE (i.e., the highest CPUE in Q4, see **Fig 4**) and that resulted in the substantial changes in the annual CPUEs (**Fig. 3**).

The annual trends of the selected model (M-3) suggested that the abundance indices of shortfin mako continuously increased from 1994 to 2014 (**Fig. 2**). Thereafter the abundance indices decreased until 2020 and increased in recent years. In consideration with a low productivity of shortfin mako due to slow growth, late maturity, low fecundity, and low steepness (Semba et al. 2009, 2011; Kai, 2019), the annual abundance index of shortfin mako estimated in the previous analysis was unreasonable due to steep increasing trend from 1994 to 2016 (Kai, 2017). However, this study indicated that spatiotemporal GLMM could slow down the steep increasing trend of this index for 1994-2016 (**Fig. 3**). Although, shortfin mako shark is known to be vulnerable to high pressure of fisheries because of a low productivity mentioned above, the population growth rates (r = 0.064; where r is the intrinsic growth rate of natural increase per year) are plausible because the latest study of the population growth rates of shortfin mako estimated from the two-stage sex model showed a similar or higher values (a mean value of r was 0.102 with a range of minimum and maximum values of 0.007-0.318) (Yokoi et al. 2017).

The year-season spatial maps showed that the hotspots of shortfin mako appeared in the vicinity of the coastal and offshore waters of Japan and the Kuroshio-Oyashio transition zone (TZ) (**Figs. 5-7**). These results supported the previous study (Kai et al., 2017a). These hotspots may be mainly formed by juvenile and subadults shortfin mako because shortfin mako is known to born during late autumn and winter off the coast of north-eastern Japan, an area known to have relatively high productivity compared with other pelagic areas, and

gradually expanded their habitat eastward and northward with the seasons as they grew (Kai et al. 2015).

The hotspots of shortfin mako were substantially changed by year (**Figs. 8**), while those were not largely changed by season (**Fig. 9**). These results suggested that the year-season effects should be considered when the spatiotemporal distribution patterns of the shortfin mako are investigated. Kai et al. (2017a) indicated that shortfin mako distribution changes seasonally with clear north-south movement, which follows higher sea surface temperatures (SST). Suppose that the shortfin mako preferred to staying in the water of higher temperature, the hotspots must be seen in the southern water in spring (Q1). A length disaggregated spatiotemporal GLMM showed that most hotspots for "immature" shortfin mako occurred in the coastal waters of Japan, while hotspots for "subadult and adult" occurred in the offshore or coastal waters of Japan (Kai et al. 2017b). Although we understand that it is very difficult to collect enough length data in addition to the catch information for this type of analysis, such model can produce the age-specific annual CPUE as well as age-specific spatial-temporal distribution maps. Further analyses considering the covariates of environmental effect and body size are needed to clarify the mechanism of seasonal changes in the spatiotemporal distribution of shortfin mako in future study.

References

Akaike, H. (1973) Information theory and an extension of the maximum likelihood principle. *In* Petrov, B.N., Csaki, F. (Eds.) Second International Symposium on Information Theory, Budapest, Akademiai Kiado, pp 267-281.

Dunn, K. P., and Smyth, G. K., 1996. Randomized quantile residuals. J. Comput. Graph. Stat. **5**, 236-244.

Hiraoka, Y., Kanaiwa, M., Ohshimo, S., Takahashi, N., Kai, M., Yokawa, K. 2016. Relative abundance trend of the blue shark *Prionace glauca* based on Japanese distant-water and offshore longliner activity in the North Pacific. Fish. Sci. 82, 687−699.

ISC. 2018. Stock assessment of shortfin mako shark in the North Pacific Ocean through 2016. ISC18-Plenary Report and Documents.

Kai, M., Shiozaki, K., Semba, Y., and Yokawa, K. 2015. Estimation of growth curve from length composition of juvenile shortfin mako, *Isurus oxyrinchus*, in the western and central north Pacific Ocean. Mar. Freshwater Res. 66: 1176–1190.

Kai, M., Shiozaki, K. 2016. Update of Japanese abundance indices for blue shark caught by Japanese offshore and distant water shallow-set longliner in the North Pacific. ISC/16/SHARKWG-1/10.

Kai, M. 2017. Updated CPUE of shortfin mako, *Isurus oxyrinchus*, caught by Japanese shallow-set longliner in the North Pacific. ISC/16/SHARKWG-1/7.

Kai, M., Thorson, J.T., Piner, K.R., Maunder, M.N., 2017a. Predicting the spatio-temporal distributions of pelagic sharks in the western and central North Pacific. Fish. Oceanogra. 26, 569−582. doi:10.1111/fog-12217.

Kai, M., Thorson, J.T., Piner, K.R., Maunder, M.N., 2017b. Spatio-temporal variation in size-structured populations using fishery data: an application to shortfin mako (*Isurus oxyrinchus*) in the Pacific Ocean. Can. J. Fish Aquat. Sci. 74, 1765−1780. doi:10.1139/cjfas-2016-0327.

Kai, M. 2019. Numerical approach for evaluating impacts of biological uncertainties on estimates of stock-recruitment relationships in elasmobranchs: example of the North Pacific shortfin mako. ICES J. Mar. Sci. 77: 200–215.

Kai, M. 2022. Spatio-temporal model for CPUE standardization: Application to blue shark caught by Japanese offshore and distant water shallow-set longliner in the western North Pacific. ISC/21/SHARKWG-2/1

Kai, M. 2023. Revisit of data filtering for CPUE of shortfin mako, *Isurus oxyrinchus*, caught by Japanese shallow-set longliner in the North Pacific. ISC/24/SHARKWG-1/1

Linden, A., Māntyniemi, A., 2011. Using the negative binomial distribution to model overdispersion in ecological count data. Ecology 92, 1414–1421. https://doi.org/10.1890/10-1831.1.

Schwarz, G. E. (1978). Estimating the dimension of a model. Annals of Statistics, 6, 461-464.

Semba, Y., Nakano, H., and Aoki, I. 2009. Age and growth analysis of the shortfin mako, *Isurus oxyrinchus*, in the western and central North Pacific Ocean. Environ. Biol. Fish. 84: 377–391.

Semba, Y., Aoki, I., and Yokawa, K. 2011. Size at maturity and reproductive traits of shortfin mako, *Isurus oxyrinchus*, in the western and central North Pacific Ocean. Mar. Freshwater Res. 62: 20–29.

Shono, H. 2005. Is model selection using Akaike's information criterion appropriate for catch per unit effort standardization in large samples? Eish. Sci. 71: 978−986.

Thorson, J.T., Fonner, R., Haltuch, M.A., Ono, K., and Winker, H. 2017. Accounting for spatiotemporal variation and fisher targeting when estimating abundance from multspecies

fishery data. Can. J. Fish Aquat. Sci. 74: 1794−1807.

Thorson, J.T. 2019. Guidance for decisions using the Vector Autoregressive Spatio-Temporal (VAST) package in stock, ecosystem, habitat and climate assessments. Fish. Res. 210, 143−161.

Thorson, J.T., Adams, C.F., Brooks, E.N., Eisner, L.B., Kimmel, D.G., Legault, C.M., Rogers, L.A., and Yasumiishi, E.M. 2020. Seasonal and interannual variation in spatio-temporal models for index standardization and phenology studies. ICES J. Mar. Sci. **77**: 1879−1892.

Yokoi, H., Ijima, H., Ohshimo, S., and Yokawa, K. 2018. Impact of biology knowledge on the conservation and management of large pelagic sharks. Scientific Reports, 7: 10619.

Tables

Table 1. Summary of model structure and outputs among different models. All models include fixed effects. "Δ" denotes a difference between the value of criteria and the minimum value for AIC and BIC.

Model	Catch rate predictors of random effect	Number of parameters	Deviance	ΔAIC	ΔBIC	Maximum gradient
M-1	Year-season and station	9	419370	388	135	< 0.0001
M-2	Year-season and station + Station	10	419320	339	96	< 0.0001
M-3	Year-season and station + Station + Season and station	14	419177	204	0	< 0.0001
M-4	Year-season and station + Station + Year and station	39	419076	154	192	< 0.0003
M-5	Year-season and station +Station + Year and station + Season and station	43	418914	0	77	< 0.003

Table 2. List of all parameters and estimates of the selected model.

No	Parameter name	Symbol	Type	Estimates
1	Distance of correlation (Spatial random effect)	κ	Fixed	0.0036
2	Northings anisotropy	h_1	Fixed	1.52
3	Anisotropic correlation	h_2	Fixed	1.01
4	Parameter governing pointwise variance (Spatial random effect)	η_{γ}	Fixed	0.84
5	Parameter governing pointwise variance (Spatio-temporal (season) random effect)	η_{ω}	Fixed	0.43
6	Parameter governing pointwise variance (Spatio-temporal (year) random effect)	η_{δ}	Fixed	No estimation
7	Parameter governing pointwise variance (Spatio-temporal (year-season) random effect)	η_{θ}	Fixed	0.35
8	Parameter governing autocorrelation (Spatio-temporal: year-season random effect)	ρ_{θ}	Fixed	1.38
9	Residual variation 1 of negative binomial model	σ_1	Fixed	1.47
10	Residual variation 2 of negative binomial model	σ_2	Fixed	0.35
11	Intercept for first predictor	β_1	Fixed	20.02
12	Intercept for second predictor	β_2	Fixed	0.0004
13	Intercept of season main effect for season 2 relative to season 1	τ_1	Fixed	1.15
14	Intercept of season main effect for season 3 relative to season 1	τ_2	Fixed	1.09
15	Intercept of season main effect for season 4 relative to season 1	τ_3	Fixed	1.41
16	Spatial residuals	γ	Random	Not shown
17	Spatio-temporal (season) residuals	ω	Random	Not shown
18	Spatio-temporal (year) residuals	δ	Random	No estimation
19	Spatio-temporal (year-season) residuals	θ	Random	Not shown

Table 3. Summary of annual CPUE predicted by spatio-temporal model along with corresponding estimates of the coefficient of variation (CV), annual nominal CPUE, and number of hooks in millions. CPUEs are predicted using the best fitting model and scaled by the average CPUE.

Year	Predicted CPUE	Nominal CPUE	CV	Number of hooks (millions)
1994	0.41	0.16	0.25	20.5
1995	0.51	0.22	0.23	18.1
1996	0.65	0.31	0.20	19.3
1997	0.63	0.43	0.19	18.0
1998	0.65	0.45	0.17	18.2
1999	0.66	0.53	0.17	20.1
2000	0.65	0.62	0.16	23.3
2001	0.73	0.54	0.15	22.9
2002	0.66	0.52	0.16	20.4
2003	0.75	0.63	0.13	18.0
2004	0.81	0.67	0.14	18.3
2005	0.96	0.89	0.12	16.6
2006	1.00	0.90	0.13	16.1
2007	1.06	0.96	0.12	18.2
2008	0.91	0.85	0.14	15.8
2009	1.21	1.13	0.12	14.4
2010	1.14	1.03	0.13	13.8
2011	1.30	1.34	0.15	7.5
2012	1.40	1.36	0.15	9.2
2013	1.16	0.95	0.16	9.5
2014	1.56	1.39	0.15	9.8
2015	1.52	1.65	0.15	8.1
2016	1.42	2.16	0.16	7.8
2017	1.40	1.73	0.17	7.3
2018	1.39	1.82	0.19	7.6
2019	1.24	1.71	0.18	7.2
2020	0.98	1.05	0.18	7.6
2021	1.10	1.07	0.18	5.7
2022	1.15	1.95	0.18	3.9

Figures

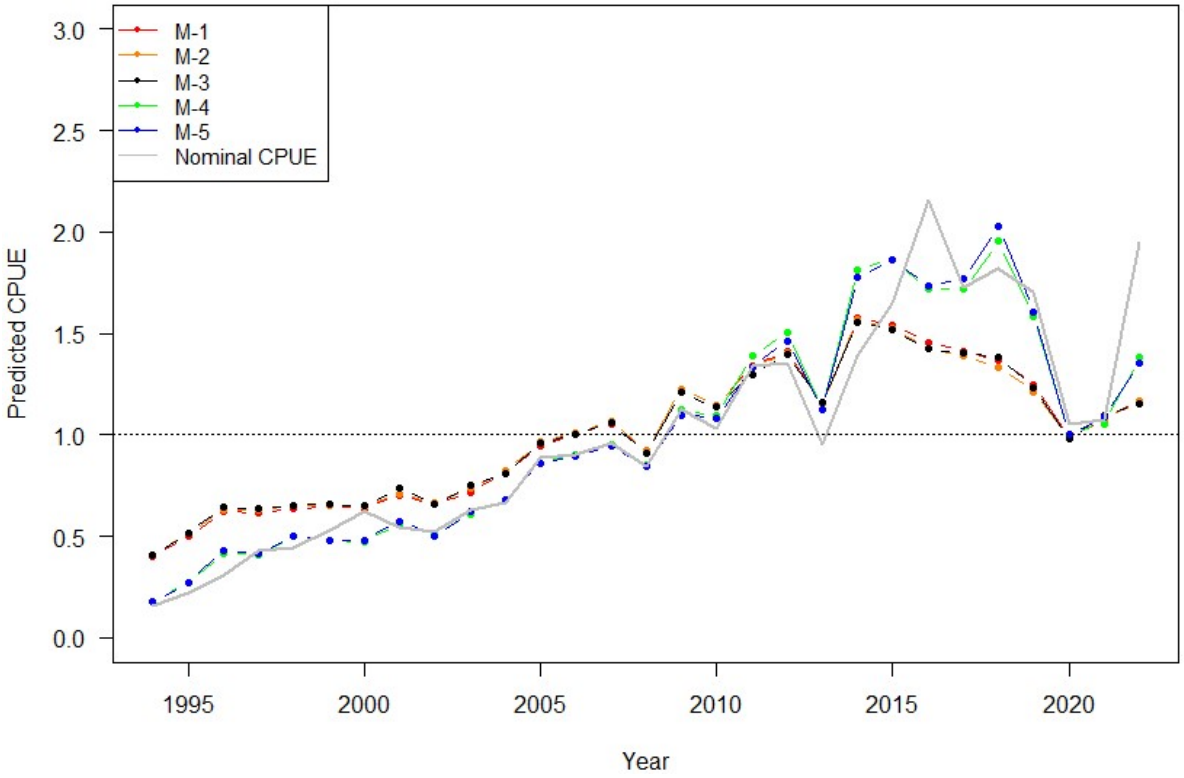

Fig. 1 Comparisons of annual predicted CPUE relative to its average among different model structures. For the details of the models, see table 1. The horizontal dotted line denotes mean of relative values (1.0).

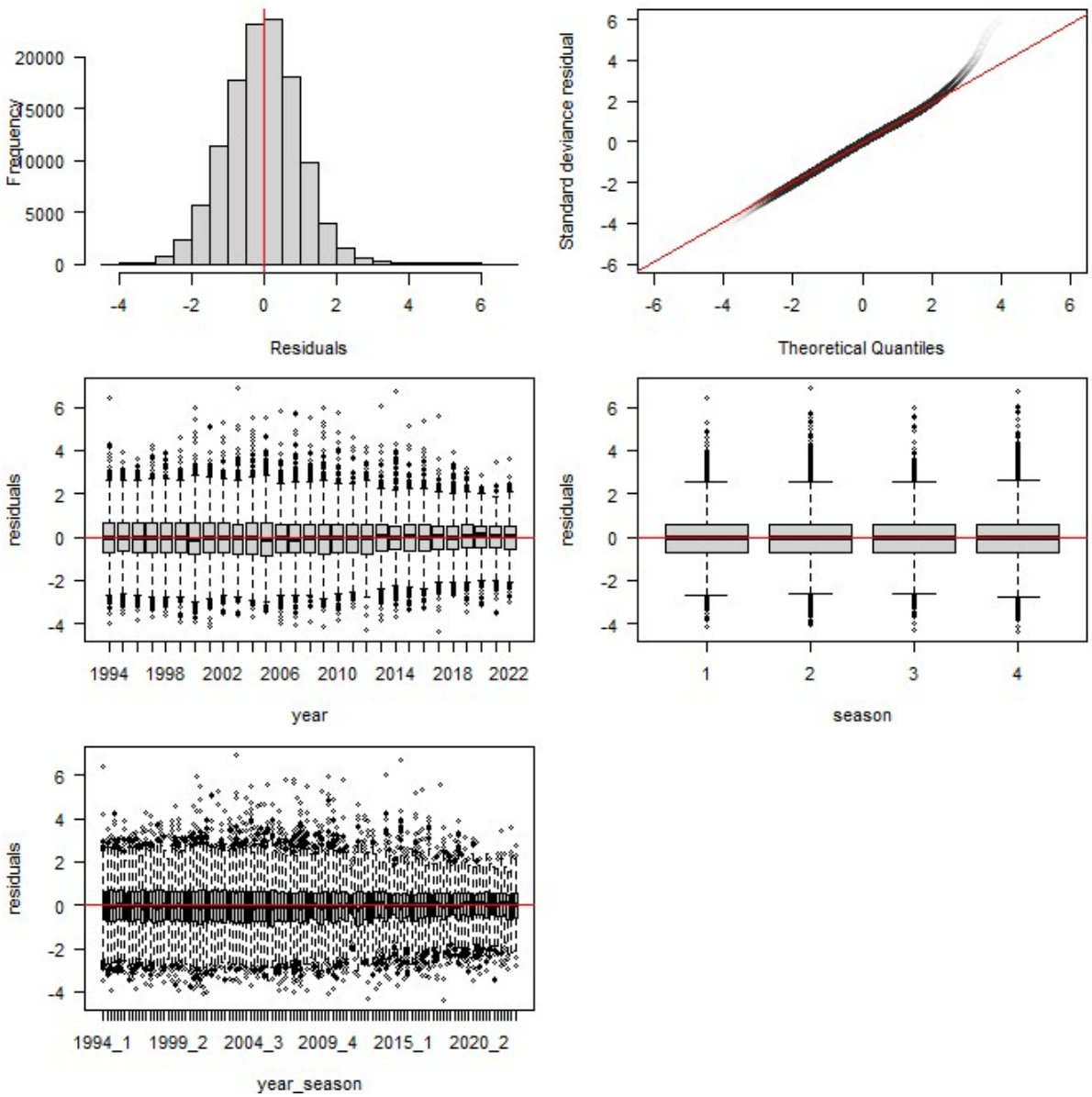

Fig. 2 Diagnostic plots of goodness-of-fit for the most parsimonious model (M-3).

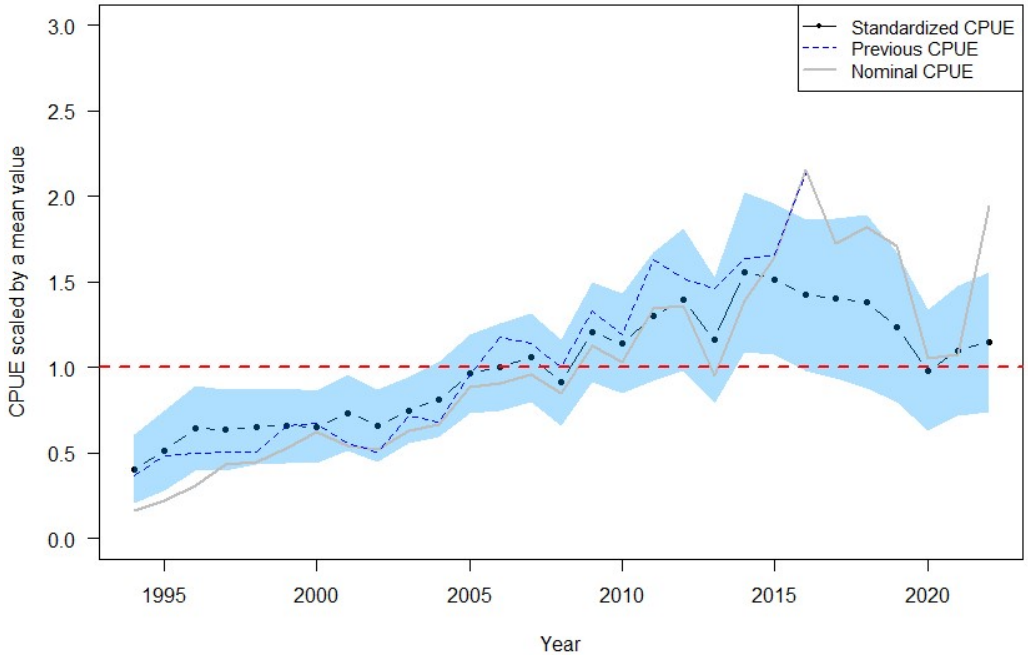

Fig. 3 Annual predicted CPUE relative to its average of the best model (M-3). Gray solid line denotes nominal CPUE relative to its average, shadow denotes 95% confidence intervals, blue dotted line denotes standardized CPUE provided in the previous assessment and horizontal dotted line denotes mean of relative values (1.0).

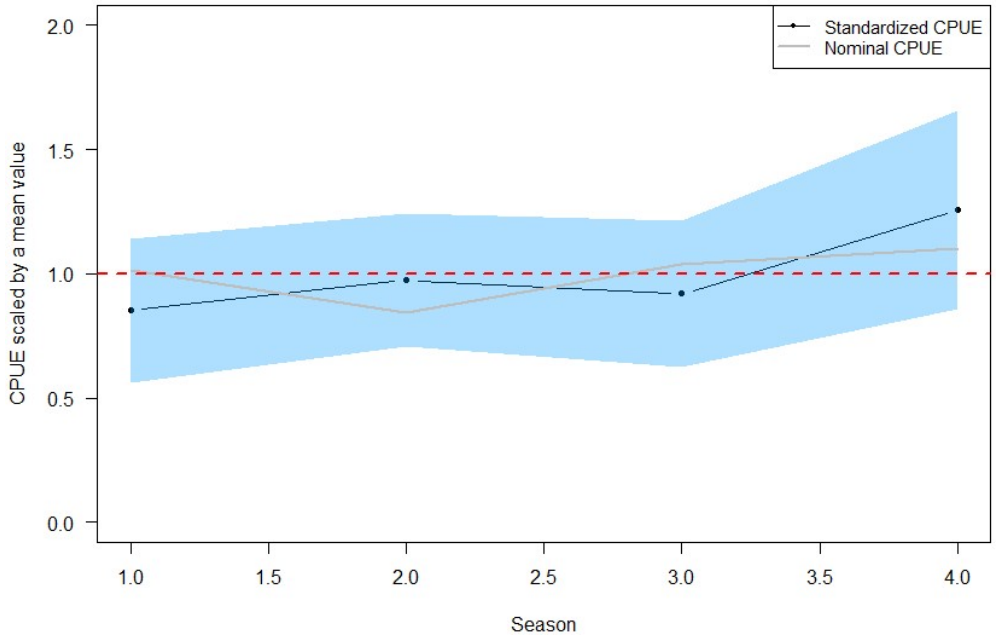

Fig. 4 Seasonal predicted CPUE relative to its average. Gray solid line denotes nominal CPUE relative to its average, shadow denotes 95% confidence intervals, and horizontal dotted line denotes mean of relative values (1.0).

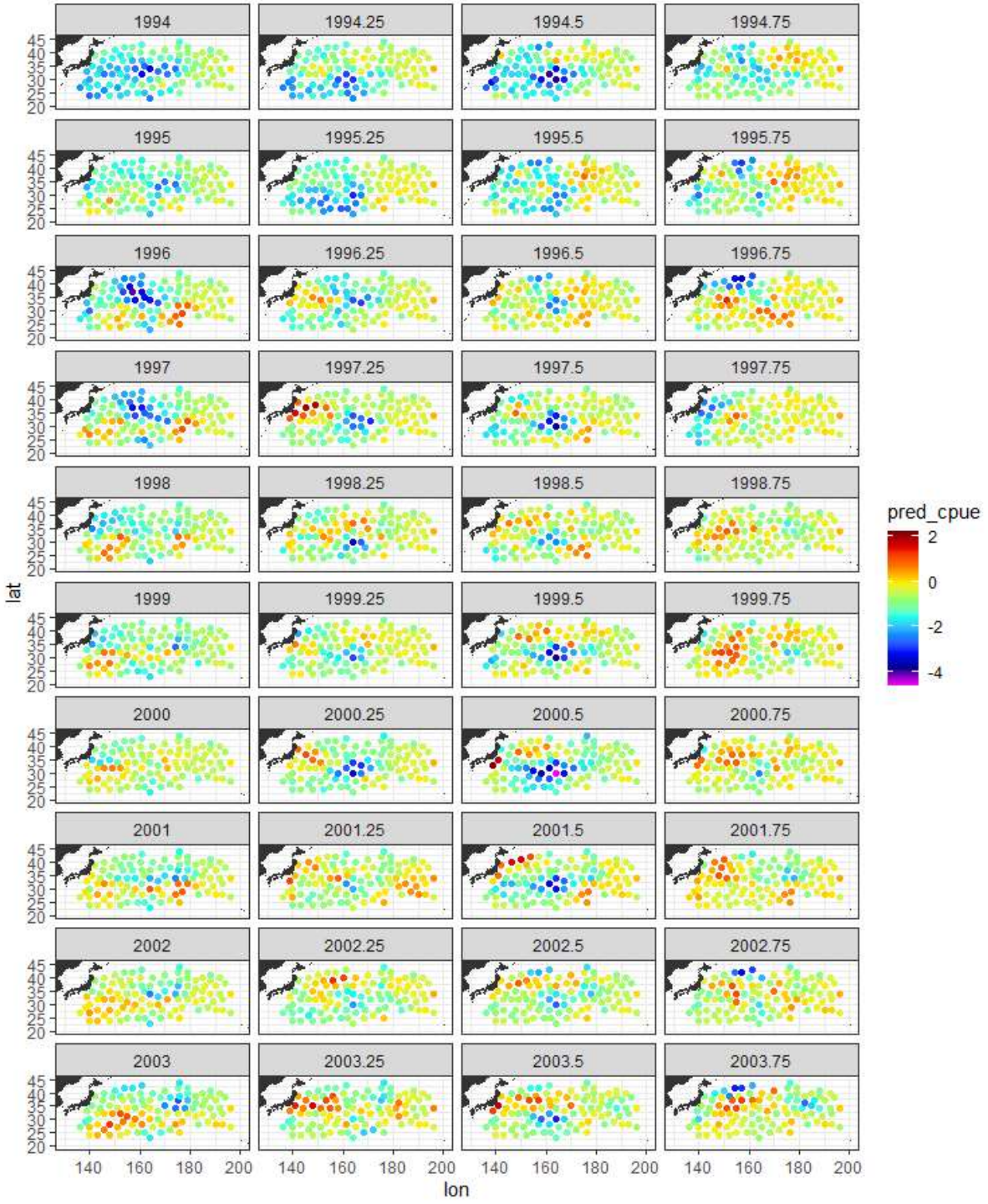

Fig. 5 Year- and season- specific spatial distribution of log-scaled predicted CPUE for shortfin mako from 1994 to 2003. Each point denotes the location of knot.

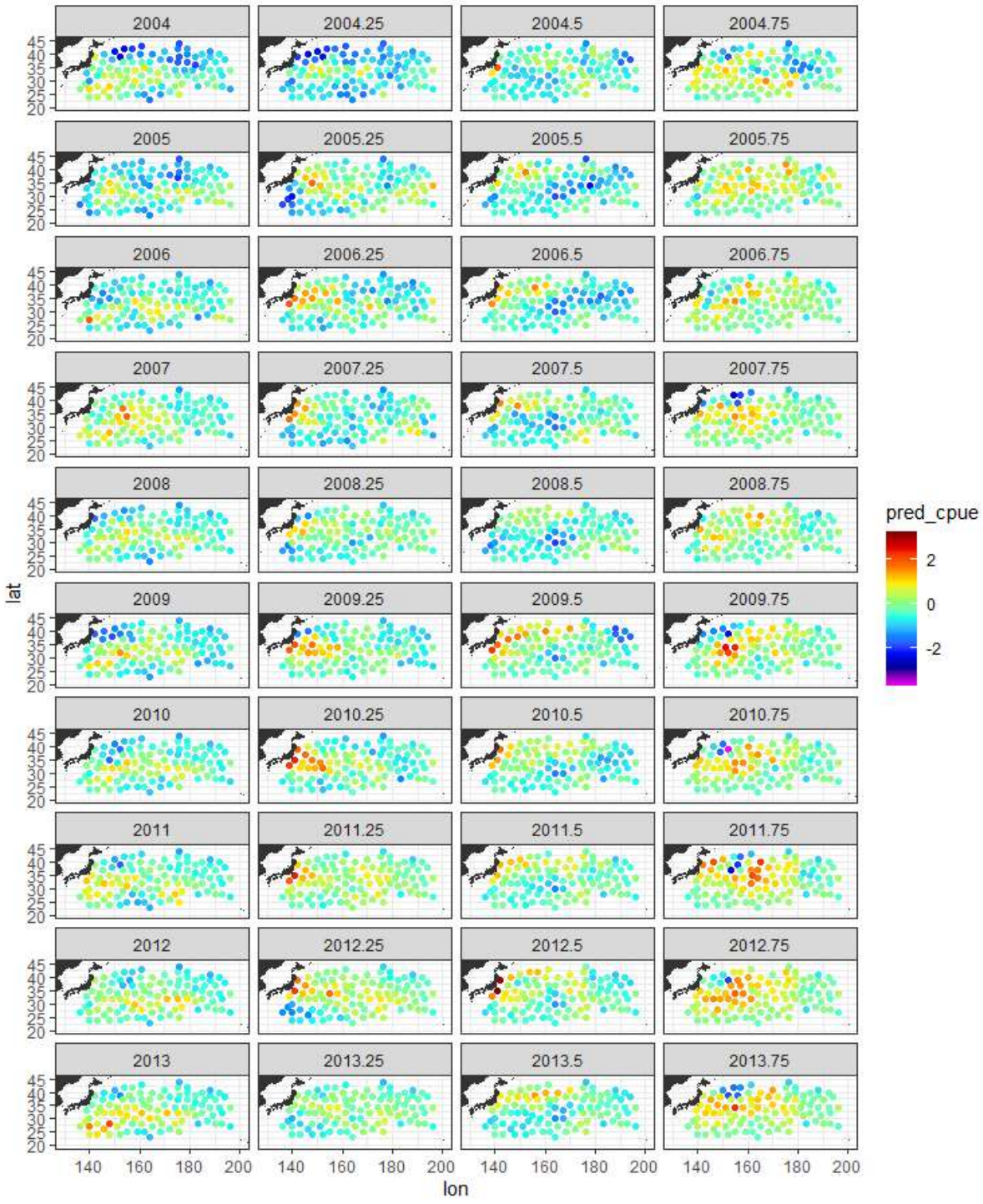

Fig. 6 Year- and season- specific spatial distribution of log-scaled predicted CPUE for shortfin mako from 2004 to 2013. Each point denotes the location of knot.

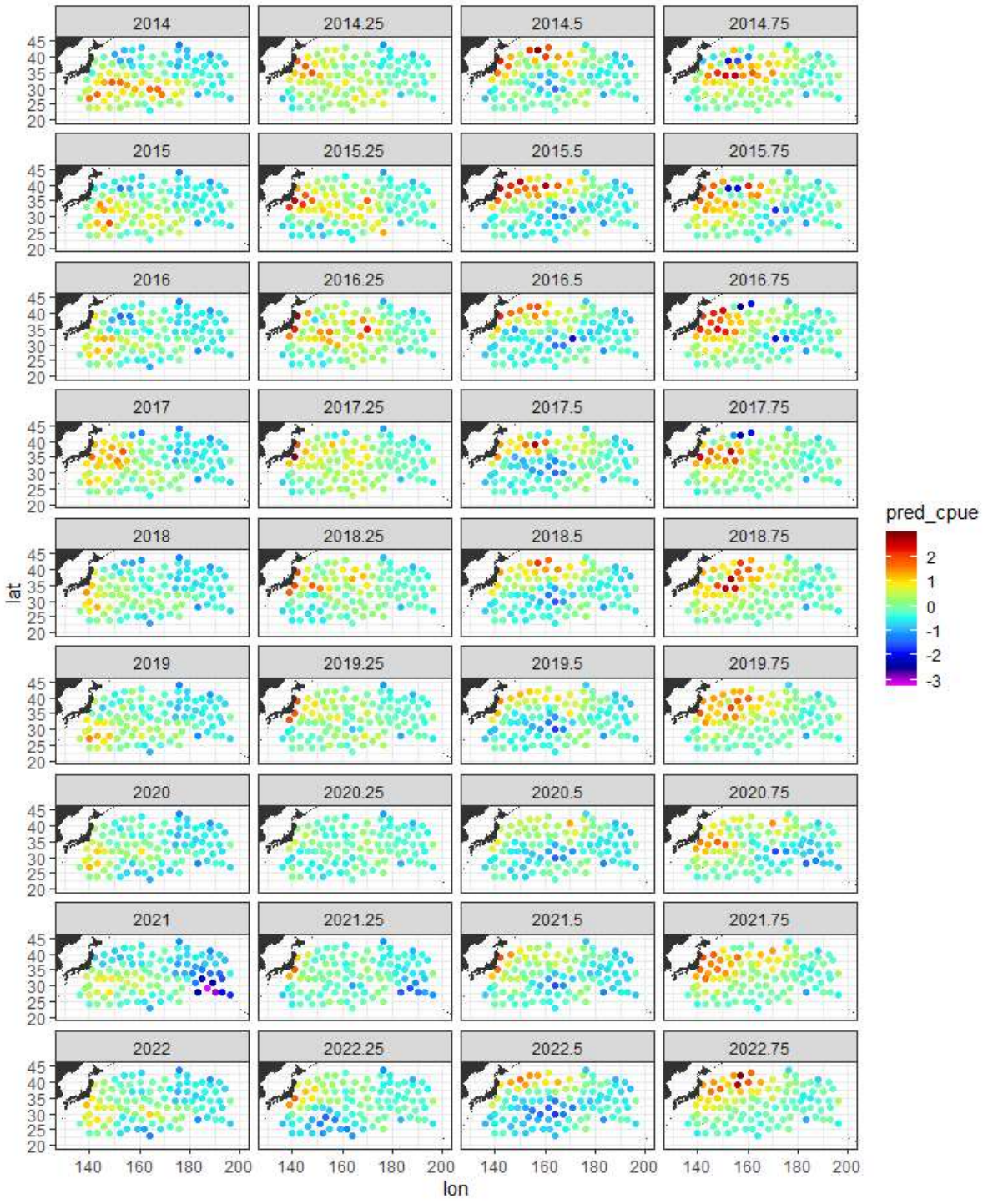

Fig. 7 Year- and season- specific spatial distribution of log-scaled predicted CPUE for shortfin mako from 2014 to 2022. Each point denotes the location of knot.

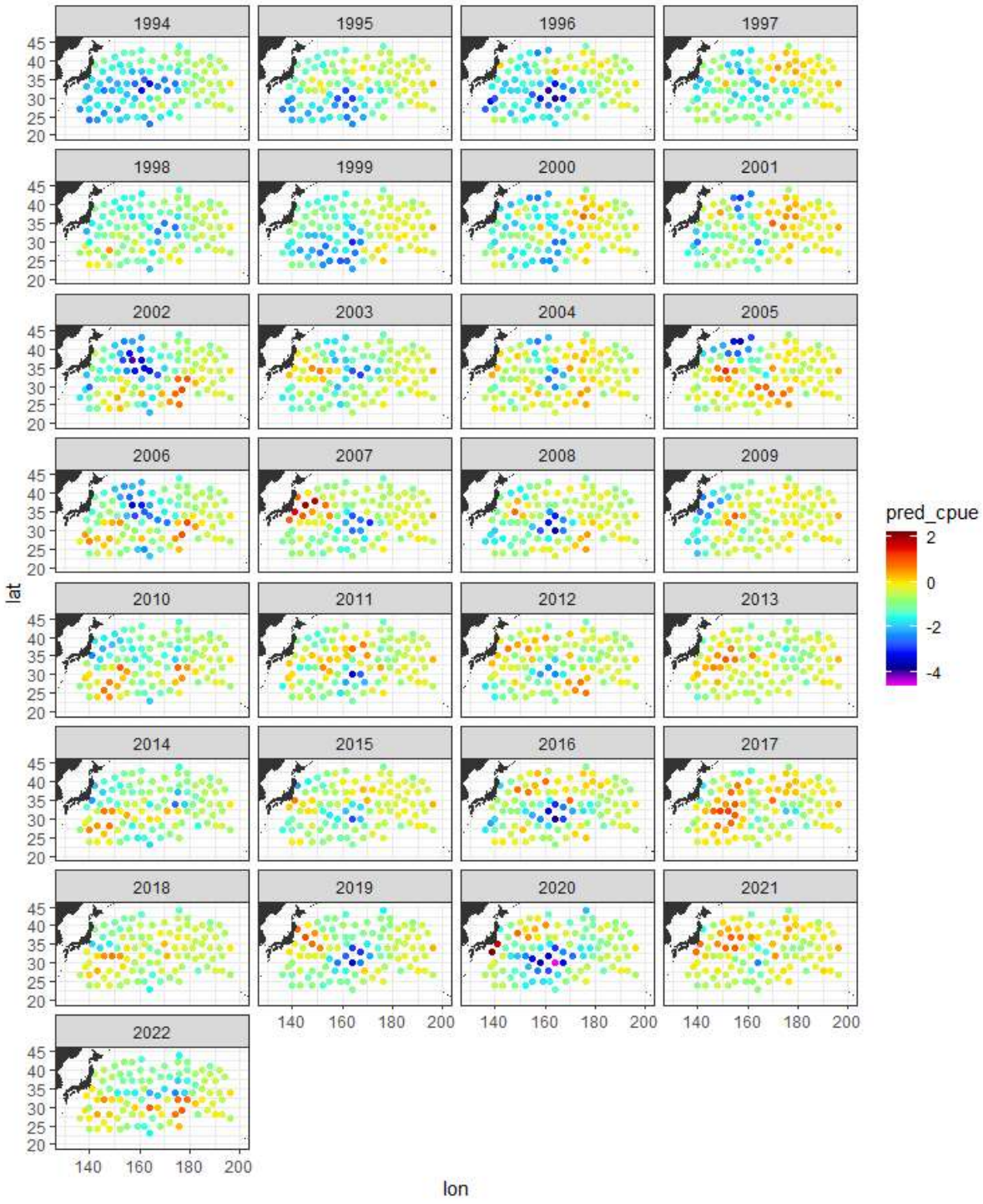

Fig. 8 Year specific spatial distribution of log-scaled predicted CPUE for shortfin mako from 1994 to 2022. Each point denotes the location of knot.

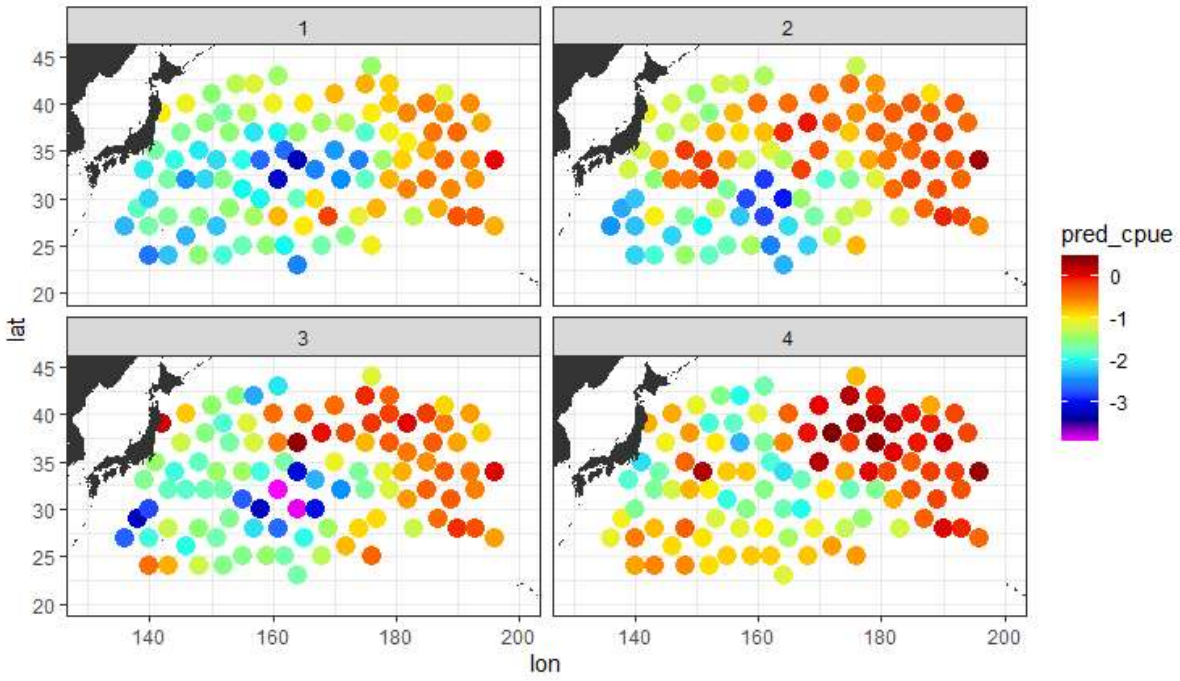

Fig. 9 Season specific spatial distribution of log-scaled predicted CPUE for shortfin mako for three month four seasons. Each point denotes the location of knot.

Appendix

Temporal (year-season) changes in the distribution shift, range expansion, and predicted CPUEs

The temporal changes in the location in Eastings and Northings indicated periodic fluctuations (**Fig. A1**). The centroid of the population's distribution shifted from southwest to northeast in Q1 and Q2 and vice-verse in Q3 and Q4. These results are synchronized with the movements of the Japanese shallow-set longliner who seasonally changes their operational areas in accordance with the target shift from swordfish to blue shark and vice versa (Hiraoka et al., 2016; Kai and Shiozaki, 2016; Kai 2021). For the eastings, the centroid of the population's distribution clearly showed a substantial change in the locations toward the western water after tsunami attack on March 11th, 2011 (**Fig. A1**) because Japanese shallow-set longliner changed their operational area from far-seas to the coastal and offshore areas off Japan in this period because of the disaster. Meanwhile, the temporal changes in the location in Northings (**Fig. A1**) indicated that the centroid of the population's distribution gradually shifted from south to north in 1990s. These results suggested that the Japanese shallow-set longliner changed their main operational area from south to north in accordance with the target shift to blue sharks due to high demands of Asian market of shark's meats and fins in 1990s and 2000s.

The temporal changes in the effective area occupied showed periodic fluctuations (**Fig. A2**). Overall, the range expansion was remarkable in Q1, while the range contraction was remarkable in Q4. Notable, the large range contractions were observed in Q4 in 2006, 2010, and 2016. However, the reasons for the sharp decline were unclear.

The temporal changes in the predicted CPUE indicated periodic fluctuations (**Fig. A3**). The highest CPUE was Q2. This result is reasonable because the Japanese shallow-set longliner changes their target species from swordfish to blue shark from Q1 to Q2.

Appendix figures

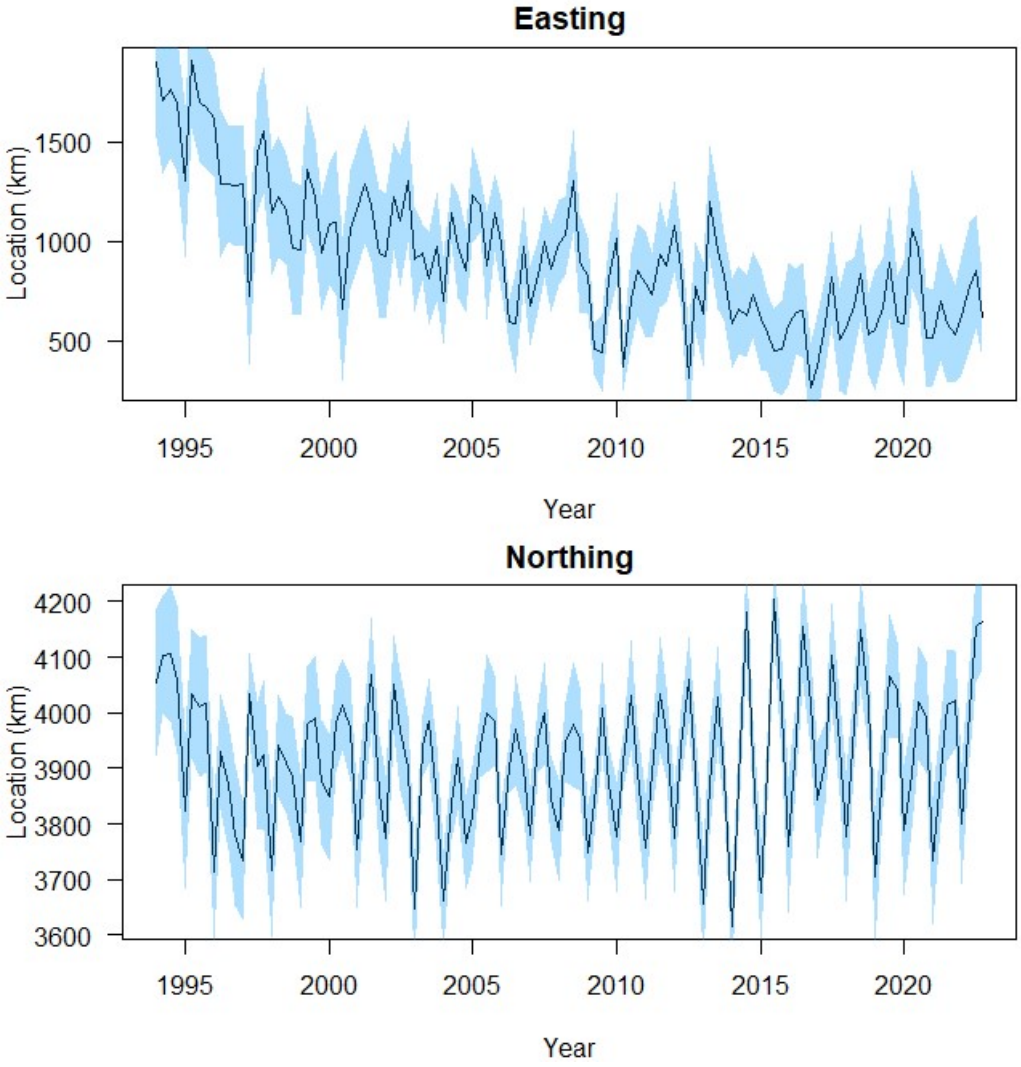

Fig. A1 Year-season changes in the centroid of the population's distribution (location in Eastings and Northings of each knot) for 1994-2022 with 95% confidence intervals (light blue shades). Upper panel denotes the movement of East-West and lower panel denotes the movement of North-South.

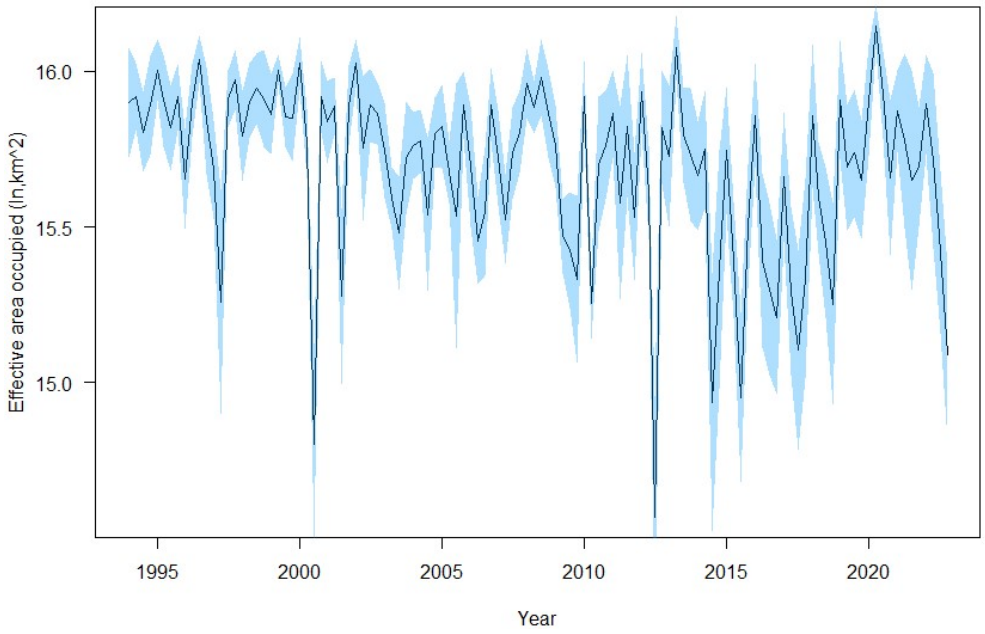

Fig. A2 Year-season changes in the effective area occupied for 1994-2022 with 95% confidence intervals (light blue shades).

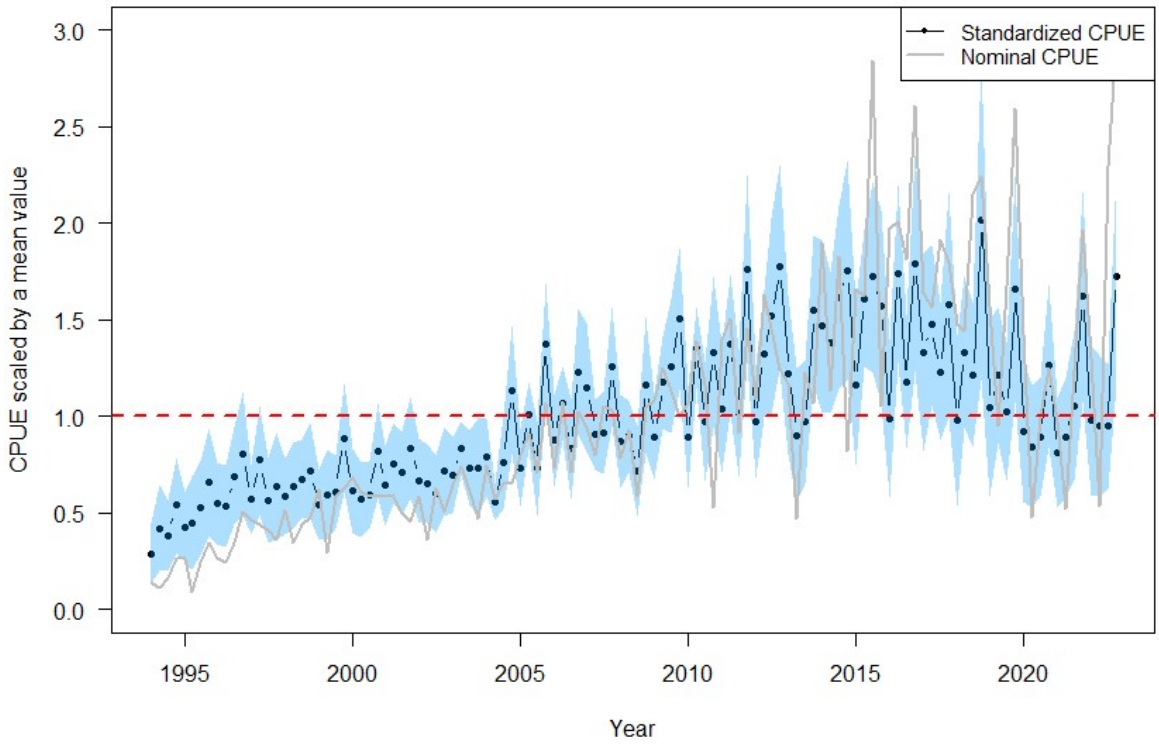

Fig. A3 Year-season changes in the predicted CPUE relative to its average. Gray solid line denotes nominal CPUE relative to its average, shadow denotes 95% confidence intervals, and horizontal dotted line denotes mean of relative values (1.0).